Inhibiting fibronectin assembly in the breast tumor microenvironment increases cell death and improves response to doxorubicin

Metti K. Gari, Hye Jin Lee, David R. Inman, Brian M. Burkel, Margaret A. Highland, Glen S. Kwon, Nikesh Gupta, and Suzanne M. Ponik

Abstract

Purpose: Effective therapies for solid tumors, including breast cancers, are hindered by several roadblocks that can be largely attributed to the fibrotic extracellular matrix (ECM). Fibronectin (FN) is a highly upregulated ECM component in the fibrotic tumor stroma and is associated with poor patient prognosis. This study aimed to investigate the therapeutic potential of an anti-fibrotic peptide that specifically targets FN and blocks the fibrillar assembly of FN.

Methods: To target FN, we used PEGylated Functional Upstream Domain (PEG-FUD), which binds to the 70 kDa N-terminal region of FN with high affinity, localizes to mammary tumors, and potently inhibits FN assembly in vitro and in vivo. Here, we used the 4T1 tumor model to investigate the efficacy and mechanisms of PEG-FUD to inhibit tumor growth.

Results: Our data demonstrates that PEG-FUD monotherapy reduces tumor growth without systemic toxicity. Analysis of the tumor microenvironment revealed that PEG-FUD effectively inhibited FN matrix assembly within tumors and reduced adhesion-mediated signaling through α5 integrin and FAK leading to enhanced tumor cell death. Notably, signaling through FAK has been associated with resistance mechanisms to doxorubicin (DOX). Therefore, we tested the combination of PEG-FUD and Dox, which significantly reduced tumor growth by 60% compared to vehicle control and 30% compared to Dox monotherapy.

Conclusions: Our findings demonstrate that PEG-FUD significantly modifies the peritumoral ECM of breast cancer, leading to increased tumor cell death, and potentiates the efficacy of conventional breast cancer therapy.

Keywords: Fibronectin, tumor microenvironment, adhesion signaling, breast cancer therapy, Doxorubicin

Introduction

Therapies for solid tumors, including breast cancer, are hindered by several roadblocks that can be largely attributed to the fibrotic ECM in the microenvironment of these tumors. The fibrotic ECM in the breast tumor microenvironment (TME) is well-known for promoting tumor aggressiveness, metastatic progression, and mechanisms of therapy resistance(1–3). During tumor progression, the deposition of ECM proteins such as collagen and FN is significantly increased, which results in tumor fibrosis. Importantly, the excess deposition of ECM in the breast TME along with alterations in ECM architecture are associated with poor breast cancer patient outcome(4–9). Based on the abundance of ECM in solid tumors and the importance of the fibrotic ECM in breast cancer progression, multiple efforts have been made to therapeutically target the ECM. To date, ECM targeting strategies have focused on interfering with ECM-modulating enzymes or signaling pathways involved in the deposition, degradation, and remodeling of ECM components (10–13). Despite the promising pre-clinical success of existing ECM-targeting drugs, most fail to transition to the clinic due to toxicity and off-target effects(14–17). Hence, there is a need to develop new therapies that specifically target the ECM and are potent enough to achieve efficacy while maintaining safety.

In this study, we focus on directly targeting FN, one of the major ECM proteins identified in the fibrotic tumor matrix(18–20). FN is a multifunctional glycoprotein that exists in two major forms, plasma FN secreted from the liver and cellular FN that is secreted locally by various cell types (21). Despite the source, FN is secreted as a soluble dimer in a compact inactive state, where it can

65 be incorporated into an insoluble fibrillar matrix upon binding to cell surface receptors, including
66 the integrin receptor α5β1(22). The N-terminal 70-kDa region of FN is required for the assembly
67 of FN into an insoluble fibrillar matrix(23). Insoluble or assembled FN matrix in the TME plays a
68 crucial role in scaffolding other ECM proteins, stabilizing the ECM, and providing adhesion sites
69 to initiate tumor cell signaling cascades that enhance proliferation and viability(24–26). To
70 specifically target FN and block the fibrillar assembly of FN, we chose to use the small 6-kDa
71 bacterial-derived peptide called Functional Upstream Domain (FUD/pUR4) discovered by
72 Tomasini-Johansson et al(27). FUD binds to the N-terminal 70-kDa region of both sources of FN
73 (cellular and plasma) with nanomolar binding affinity, consequently, blocking the extension of FN
74 and assembly into fibrils(27). Importantly, FUD is a potent inhibitor of FN assembly both *in vitro*
75 and *in vivo*(28–30). Several laboratories have demonstrated the potential of FUD as a therapeutic
76 agent in multiple fibrotic diseases, including breast cancer(31). However, the peptide is rapidly
77 cleared through the renal system, which limits the *in vivo* bioavailability and results in daily
78 required FUD administration at a relatively high dose of ~25 mg/kg(32). To address the issue of
79 rapid renal clearance, we PEGylated-FUD (PEG-FUD) and demonstrated a significant increase in
80 peptide bioavailability and tumor retention compared to non-PEGylated FUD, while maintaining
81 the ability to inhibit FN assembly(33–36).

82 Here, we investigated the anti-cancer efficacy of PEG-FUD in the TNBC 4T1 mouse mammary
83 carcinoma model. We hypothesized that modulating FN assembly into a fibrillar matrix with PEG-
84 FUD would disrupt cell-ECM interactions thereby inhibiting tumor growth, blocking mechanisms
85 of drug resistance, and improving the efficacy of chemotherapy. Our study revealed that treatment
86 with PEG-FUD significantly decreased 4T1 tumor growth. By characterizing the alterations in the
87 TME in response to PEG-FUD, we identified a significant inhibition of FN matrix assembly,

88 reduced levels of cell adhesion proteins (including α5 integrin and FAK), and an increase in
89 caspase-3 mediated cell death. Further investigation into the potential of PEG-FUD to improve
90 chemotherapy response revealed that co-treatment with PEG-FUD significantly enhanced the anti-
91 tumor efficacy of Dox without any additional systemic toxicity.

92

93 ## Materials and Methods

94 **Preparation of Functional Upstream Domain (FUD) peptide and its mutated counterparts**

95 FUD and the FUD control (mutated FUD (mFUD) and Fully mutated FUD (FmFUD)) constructs
96 were a kind gift from Dr. Donna Peters at University of Wisconsin-Madison. The mFUD and
97 FmFUD control peptides have reduced binding affinity for FN due to point mutations in the FN
98 binding regions. All peptide sequences were cloned into the pET-ELMER vector and
99 recombinantly expressed in BL21 *Escherichia coli* (DE3) as His-tagged peptides as previously
100 described by our group(33–36). Briefly, 1 mM of isopropyl β-D-1thiogalactopyranoside (IPTG)
101 was added to the obtained 1L culture to induce expression of FUD/mFUD/FmFUD. The resulting
102 bacterial pellet was suspended in the lysis buffer (pH 8.0) [Urea 8M, NaH_2PO_4 100 mM, Tris 10
103 mM, Imidazole 5 mM] and centrifuged to obtain clear supernatant. Ni-NTA agarose (Qiagen)
104 beads were equilibrated with the lysis buffer and 1 mL of Ni-NTA agarose resin was added for
105 every 4 mL of the above obtained lysate and incubated overnight at 4°C with Ni-NTA agarose
106 beads. The next day, the lysate was removed and the Ni-NTA agarose was washed with a washing
107 buffer (pH 8.0) [Urea 8M, NaH_2PO_4 100 mM, Tris 10 mM, Imidazole 15 mM] and equilibrated
108 with Thrombin cleavage buffer (pH 8.4) [$CaCl_2$ 2.5 mM, NaCl 150 mM, Tris 20 mM]. Elution of
109 peptides and removal of the His tag was achieved by using a thrombin cleavage site between the

110 His-tag and the corresponding peptide (FUD/mFUD/FmFUD). FUD bound to the Ni-NTA agarose
111 was incubated with ~36 units of Bovine α-Thrombin for every 15 mL of sample. The eluted sample
112 was collected and further purified via fast protein liquid chromatography (FPLC) using HiTrap Q
113 HP column from Cytiva.

114

115 **PEGylation of FPLC purified peptides**

116 PEGylated conjugates were synthesized using reductive amination chemistry. FUD, mFUD or
117 FmFUD peptide(s) were N-terminally selectively conjugated with 20-kDa methoxy-PEG-
118 propionaldehyde using the previously published protocol by our group(33). Briefly, the FPLC
119 purified FUD/mFUD/FmFUD peptide was mixed with PEG in a sodium acetate buffer solution
120 (50 mM, pH 5.5) in the presence of $NaBH_3CN$ and the reaction was carried out for ~18 hr in the
121 fuming cabinet under cold conditions (4°C). After the reaction time was complete, the mixture was
122 dialyzed two times against NaOAc buffer to remove excess reducing agent. Next, the buffer was
123 switched to 20mM Tris and left overnight before FPLC purification via ion-exchange
124 chromatography using 5mL HiTrap Q HP anion exchange column. The concentration of
125 FUD/mFUD/FmFUD was obtained by measuring the absorbance at 280 nm using corresponding
126 ε values [0.496 (FUD), 0.742 (mFUD) and 0.250 (FmFUD)]. Patent number for PEG-FUD:
127 US10828372B2.

128

129 **Enzyme-linked competition binding assay**

130 The enzyme-linked competition binding assay was carried out as previously reported(37,38), with
131 a small modification. Briefly, a 96-well high-binding culture plate was coated overnight with

132 human plasma FN under cold conditions (4°C) at 10 μg/mL of concentration. The biotinylated
133 FUD (b-FUD) was prepared as per the manufacturer's protocol using NHS-biotin-ester (Pierce).
134 The above FN-coated plate was blocked for 1 hr using 5% BSA prepared in tris-buffered saline
135 containing 0.05% Tween 20 (TBS-T). 0.5 nM of b-FUD was added to the plate concurrently with
136 various concentration (2000, 1000, 500, 250, 125, 62.5, 0 nM) of unlabeled PEG-FmFUD or PEG-
137 FUD in 0.1% BSA in TBS-T. After a 2 hr incubation at RT, followed by three TBS-T washes,
138 alkaline phosphatase-conjugated streptavidin (Jackson Immunoresearch) was added at 1:20,000
139 dilution factor and incubated for 1 hr at RT. After washing with TBS-T again, 100 uL of 1-step p-
140 Nitrophenyl Phosphate was added as a substrate to each treated well, and the reaction was stopped
141 by the addition of 2N sodium hydroxide. Absorbance was measured at 405 nm using a microplate
142 reader.

143

144 **Cell monolayer culture**

145 4T1 breast cancer cells were obtained from American Type Culture Collection (VA). 4T1 cells
146 were cultured in Rosewell Park Memorial Institute Medium-1640 (RPMI) (Corning, NY, USA)
147 containing 10% fetal bovine serum (FBS). The human breast cancer-associated fibroblasts
148 (hCAFs) cells were a gift from Charlotte Kupperwaser's laboratory at Tufts University. The hCAFs
149 were cultured in Dulbecco's Modified Eagle Medium (DMEM, Gibco) containing 10% FBS and
150 1% streptomycin/penicillin. The bone-marrow-derived fibroblast cells isolated from the femurs of
151 BALB/c mice were cultured in DMEM containing 20% FBS and 1% streptomycin/penicillin and
152 activated by 4T1-conditioned media to generate murine cancer-associated fibroblasts (mCAFs) as
153 described previously (39). All cell cultures were kept at 37°C in the humidified incubator with 5%

154 CO_2. For tumor cell inoculations, cells were washed, harvested and counted manually using a
155 hemocytometer.

156

157 **Cell monolayer ECM staining**

158 To confirm ECM changes in fibroblast culture after PEG-FUD incubation, 25,000 hCAFs or
159 mCAFs in corresponding media containing 50 μg/ml of ascorbic acid were seeded onto a 35 mm
160 glass bottom dish (VWR). The next day, 250 nM of PEG-FUD peptides in phosphate-buffered
161 saline (PBS) were incubated with hCAFs or 500 nM of PEG-FUD was incubated with mCAFs for
162 48 hr. PBS was used as a vehicle in control groups. After the peptide incubation, cells were washed
163 with Hanks' Balanced Salt Solution and fixed with 10% formalin for 10 min at RT. Following
164 fixation, 2% BSA in PBS was used for blocking for 1 hr at RT. hCAFs were incubated with a
165 A488-labeled anti-FN primary antibody (eBioscience, No. 53-9869-82, 1:100) in 1% BSA/PBS at
166 4°C overnight. The next day, cells were washed to remove unbound primary antibody. mCAFs,
167 were immunolabeled using a rabbit anti-mouse FN primary antibody (1:500) (34) in 1% BSA/PBS
168 at 4°C overnight and an A488-labeled goat anti-rabbit (Life technologies, A11034, 1:500)
169 secondary antibody in 1% BSA in PBS for 1 hr at RT. After washing, nuclei were stained with
170 DAPI (D9542, MilliporeSigma). Confocal microscopy (Nikon AIRS with 20x objective lens) was
171 used to visualize the assembled FN by the fibroblasts, and images were processed with the vendor
172 software (NIS-Elements).

173

174 **Animal Tumor model**

175 9-week-old female BALB/c mice were purchased from Jackson Labs and housed in the Wisconsin
176 Institutes for Medical Research animal facilities at the University of Wisconsin-Madison. All
177 experiments were conducted in compliance with the University of Wisconsin Institutional Animal
178 Care and Use Committee (IACUC). 4T1 tumors were established by orthotopically injecting 2×10^5
179 4T1 cells in 50 µl DPBS into the fourth mammary fat pad of syngeneic, immunocompetent
180 BALB/c mice. To minimize tumor abrasion, mice were housed on soft bedding. To assess FN
181 protein levels, major organs such as the mammary glands, lungs, liver, spleen, and kidney were
182 harvested from 4T1 tumor bearing and non-tumor bearing control mice 4 weeks after 4T1 cell
183 inoculation. For PEG-FUD monotherapy, after orthotopic tumor injection, all mice were randomly
184 assigned to an experimental group. After 1 week of tumor growth, when tumor size reached
185 approximately 50 mm^3, vehicle control (Ctrl_PBS) or peptides (PEG-FmFUD, PEG-mFUD and
186 PEG-FUD) were administered subcutaneously at the scruff of the neck every 48 hr at a dose of
187 12.5mg/kg (outlined in Fig 3). For combination therapy (PEG-FUD + Dox), 4 doses of PEG-FUD
188 or control peptides were administered every 48 hrs, then Dox treatment was initiated, which
189 consisted of intraperitoneal administration every 72 hr at 5 mg/kg along with continued peptide
190 dosing every 48 hrs (outlined in Fig 7A). During the treatment course, tumor growth was measured
191 manually every 48 hr using a caliper, starting at the first treatment. Tumor volume was calculated
192 using the formula $V = ½ (Length \times Width^2)$(40). The maximal tumor volume approved by the
193 IACUC at the University of Wisconsin-Madison is 1.5 cm^3. In compliance with these guidelines,
194 all animals in this study were euthanized at or before tumors reached this volume (Supplemental
195 Table 1A-B). At the end of the treatment, blood was collected, mice were euthanized, and tissues
196 were harvested for subsequent analysis.
197

198 **Toxicity evaluation**

199 Body weight was monitored every 48 hr during the treatment course. At the experimental end
200 point, blood was collected via cardiac puncture to perform a complete blood count (CBC) analysis
201 using the VETSCAN® HM5 Hematology Analyzer. During harvest, the spleen was collected and
202 weighed. Additionally, kidneys and liver were harvested and fixed in 10% buffered formalin for
203 48 hr at 4 °C. Fixed tissues were paraffin embedded and 5 μm sections were stained with
204 hematoxylin and eosin (H&E) by routine methods. Stained slide sections were captured at 40x by
205 Aperio Digital Pathology Slide Scanner system and the digitized slides were evaluated by a board
206 certified veterinary anatomic pathologist using Aperio ImageScope [v12.4.6.5003].

207

208 **Immunofluorescence staining**

209 4T1 tumors were fixed for 48 hr at 4 °C in 10% buffered formalin. Fixed tissues were paraffin-
210 embedded and sectioned into 5 μm sections for immunofluorescence analysis. Briefly, tissue
211 sections were deparaffinized in a humidity chamber with xylene and rehydrated in graded ethanol
212 washes. Next tissue sections were subjected to heat-induced antigen retrieval in citrate buffer pH
213 6.0. Slides were blocked with 10% BSA in TBS for 1 hr then incubated for 1 hr at RT with primary
214 antibodies, FN (ab23750, Abcam, 1:250) and Antigen Kiel 67- Ki67 (ab15580, Abcam, 1:100),
215 followed by washing in TBS-T. Next, samples were incubated with secondary antibody (ab7090,
216 Abcam, 1:500) for 10 min at RT. For amplified fluorescence detection, sections were incubated
217 with TSA substrates (PerkinElmer) for 10 min at RT, followed by nuclear counterstaining with
218 DAPI (D9542, MilliporeSigma). Slides were coverslipped using ProLong Gold (no. P36930;
219 Thermofisher). Immunofluorescent labeled slides were imaged using a Leica Thunder imaging

220 system with 10x magnification. Quantification of >10 fields of view was performed in Image J for
221 each staining.
222
223 **Picro-sirius red (PSR) staining**
224 Formalin fixed paraffin embedded (FFPE) 4T1 tumor tissues were sectioned at 5 μm for PSR
225 staining. Briefly, tissue sections were deparaffinized with xylene and underwent sequential washes
226 of graded ethanol as described above. Next slides were stained with PSR (Sigma-Aldrich; "Direct
227 Red 80"; Catalog # 36-554-8) for 1 hr. Slides were then washed with acidified water, dehydrated
228 in 100 % ethanol, and cleared in xylene. Slides were coverslipped using Richard-Allan Scientific
229 Mounting Medium (REF 4112, Thermo Scientific). PSR stained slides were imaged at an
230 excitation wavelength of 575 nm using Leica Thunder imaging system with a magnification of
231 20x. Quantification of >10 fields of view were performed in Image J.
232
233 **TUNEL staining**
234 FFPE 4T1 tumor sections were deparaffinized and rehydrated as described above. Sections were
235 then stained with a 1:10 dilution of TUNEL enzyme in TUNEL buffer (Roche In Situ Cell
236 Detection Kit w/Fluorescein. Catalog # 11684795910) for 1 hr at 37°C, washed with PBST, and
237 coverslipped with ProLong Gold mounting media (no. P36930; Thermofisher). TUNEL stained
238 slides were imaged at an excitation wavelength of 475 nm using Leica Thunder imaging system
239 with a magnification of 20x.
240
241 **Western Blotting**

242 Tissues were fractionated into soluble and insoluble lysates similar to our prior study(34). Briefly,
243 tissues were cryopulverized using a mortar and pestle in the presence of liquid nitrogen. The
244 homogenized samples were lysed in RIPA buffer containing 1% deoxycholate (DOC) at 0.1 g
245 tissue per ml buffer and spun at 4°C. The supernatant was collected, and the pellets were
246 solubilized in buffer containing 4 M urea, 4% SDS and 1 mM DTT. Resuspended pellets were
247 vortexed, sonicated, and heated to 95°C for 5 min. The DOC-soluble supernatant contains nuclear,
248 cytoplasmic, and membrane fractions, while mainly ECM proteins constitute the DOC-insoluble
249 pellet. Protein concentrations were measured using the DC Protein Assay kit (Bio-Rad) and BSA
250 standards, diluted in the corresponding buffers. Proteins in each fraction were separated by SDS–
251 polyacrylamide gel electrophoresis and transferred to a polyvinylidene difluoride membrane. To
252 ensure even protein loading and transfer efficiency, total protein (TP) staining (Fast Green FCF,
253 MilliporeSigma) was performed. Next, membrane was blocked with 5% non-fat dry milk solution
254 in TBS-T, and incubated overnight at 4°C with the following primary antibodies: FN (ab23750,
255 Abcam, 1:250, 2hr); COL1A1 (NBP1-30054, Novus Biologicals, 1:500); tenascin-C (ab108930,
256 Abcam, 1:500); periostin (ab14041, Abcam, 1:500) ; proliferating cell nuclear antigen - PCNA
257 (#13110, Cell Signaling, 1:500); Caspase-3 (#9662, Cell Signaling, 1:500); integrin α5 (10569-1-
258 AP, proteintech, 1:1000); integrin β1 (#34971, Cell Signaling, 1:1000); FAK (#05-537,
259 MilliporeSigma, 1:1000). Proteins were detected using either a horseradish peroxidase–conjugated
260 secondary antibodies (Jackson ImmunoResearch) followed by chemiluminescence substrate (LI-
261 COR BioScience) or fluorescent–conjugated secondary antibodies (IRDye infrared dyes from LI-
262 COR Biosciences). Blots were imaged using the Odyssey Fc Imager and band intensities were
263 analyzed using Image studio. For detection of plasma FN, blood was isolated from mice via cardiac
264 puncture and spun for 10 min at 2,000 x-g to remove cells. Next, the plasma layer was collected

265 and spun for 15 min at 2,000 x-g to deplete platelets in the plasma. The supernatant was collected
266 and put in 2x Laemmli followed by standard procedures of Western blotting as described above.
267
268 **Statistics**
269 GraphPad Prism was used to generate graphs and perform statistical analysis. For comparison
270 between two groups, an unpaired t-test was performed. For comparison between multiple groups,
271 a one-way analysis of variance (ANOVA) with Tukey's Multiple Comparison Test (TMCT) was
272 performed, with a corrected P value ≤ 0.05 considered significant. Data is reported as mean ± s.e.m.
273

274 Results

275 **PEG-FUD inhibits mammary CAF-mediated FN assembly *in vitro***
276 Cancer-associated fibroblasts (CAF) are one of the most abundant stromal cells in the TME and
277 the primary cell type responsible for the deposition of ECM proteins, including FN. CAFs not only
278 secret FN but also assemble FN(41). We previously showed that Cy5-labeled PEG-FUD can bind
279 to exogenous or endogenous FN assembled by CAFs(36). Prior studies have shown that PEG-FUD
280 inhibits FN assembly by human foreskin fibroblasts(33,42), however, PEG-FUD has yet to be
281 demonstrated as an inhibitor of FN assembly by mammary CAFs. To confirm PEG-FUD inhibits
282 mammary CAF-mediated FN matrix assembly, we induced ECM matrix assembly in hCAFs or
283 activated mCAFs and treated cells with control (Ctrl_PBS) or PEG-FUD (250 or 500 nM,
284 respectively) for 48 hrs. At experimental endpoint, the cultures were fixed and the fibrillar structure
285 of FN was visualized by immunofluorescence staining. PEG-FUD significantly decreased the area
286 of cellular FN assembled by mCAFs (Fig 1A-B). Additionally, we identified a similar decrease in
287 hCAF-mediated fibrillar FN assembly in the presence of PEG-FUD compared to the control, PBS-

288 treated condition (Fig 1C-D). These results provide evidence that PEG-FUD broadly inhibits *in*

289 *vitro* FN assembly by fibroblasts, including FN assembled by mammary CAFs *in vitro*.

290

291 **FN is highly expressed in 4T1 mammary tumors compared to other organs**

292 FN expression is significantly increased in human breast tumors compared to normal breast tissue

293 and is correlated with poor prognosis(43,44). To investigate the therapeutic potential of PEG-FUD

294 to inhibit FN assembly, we chose the aggressive 4T1 pre-clinical murine model that mimics human

295 TNBC(45). Before testing the therapeutic efficacy of PEG-FUD, we set out to validate and

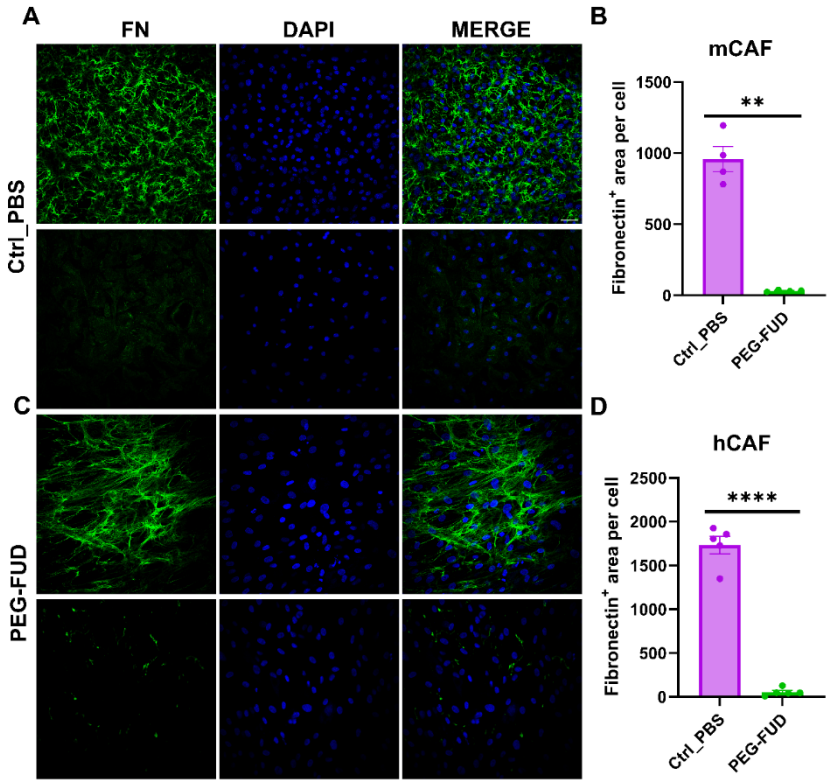

Figure 1: **Fibronectin (FN) assembly inhibition by PEG-FUD in mCAF & hCAF.** (A) Immunofluorescence staining of FN assembled by mCAF 48 hr after incubation of a vehicle control (Ctrl_PBS) or PEG-FUD (500 nM each). Scale bar = 100 µm. (B) FN (+) area changes measured by fluorescence-positive area per number of cells (nuclei). **P<0.005, n=4 per group. (C) Immunofluorescence staining of FN assembled by hCAF 48 hr after incubation of a vehicle control (Ctrl_PBS) or PEG-FUD (250 nM each). (D) FN (+) area changes measured by fluorescence-positive area per number of cells (nuclei). ****P<0.0001, n=5 per group.

296 quantify the increase in circulating and peritumoral FN in the 4T1 tumor model. To accomplish

297 this goal, we quantified FN levels in plasma and major organs of normal (non-tumor bearing) and
298 tumor-bearing mice. Plasma FN (pFN) levels were similar in normal mice and in 4T1 tumor-
299 bearing mice (Fig 2A). However, when assessing FN in major organ tissues, we found both soluble
300 FN (sFN) and assembled / insoluble FN (iFN) levels were significantly increased in tumor tissues
301 compared to all other major organs in both normal and tumor-bearing mice (Fig 2B-C).
302 Specifically, 4T1 mammary tumors had more than 20-fold higher FN than normal mammary
303 glands. Analysis of FN in the kidney, heart, liver, and spleen tissue revealed no significant
304 difference in sFN or iFN between tumor-bearing and non-tumor-bearing mice. Notably, the lung
305 tissue of 4T1 tumor-bearing mice had a trend toward increased iFN compared to the lungs of non-
306 tumor-bearing mice. Similarly, others have identified an increased accumulation of total FN in
307 metastatic 4T1 lesions isolated from multiple organ sites of tumor-bearing mice compared to non-
308 tumor-bearing normal organs(46). Overall, our results validate that 4T1 tumors are high in sFN
309 and iFN expression, making it a suitable model to study the anti-cancer effects of inhibiting FN
310 assembly with PEG-FUD.

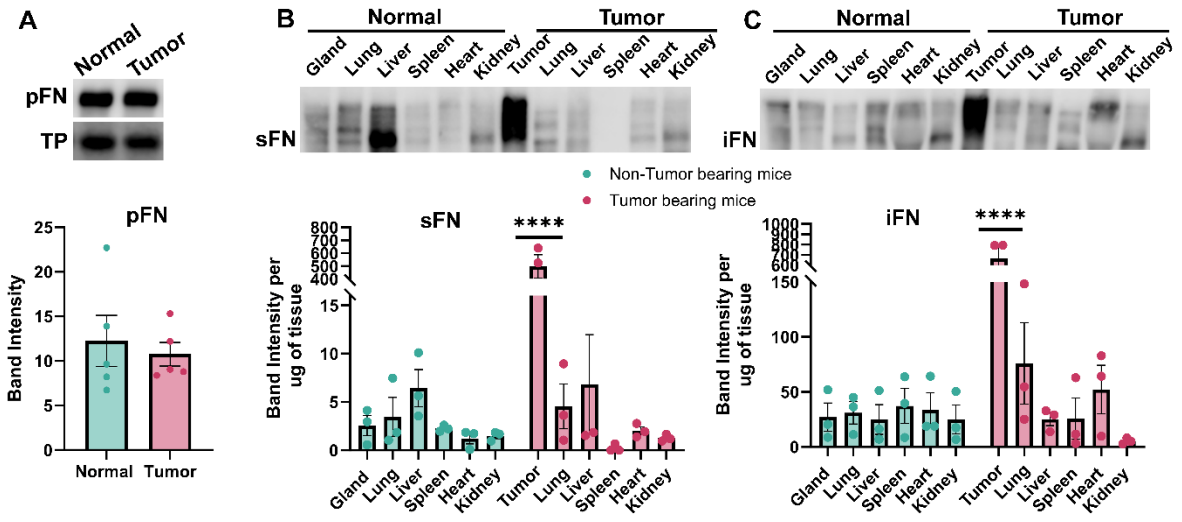

Figure 2: **High FN expression in 4T1 mammary tumors compared to other organs**. 9-week-old female BALB/c mice were injected with 2×10^5 4T1 cells into the fourth mammary fat pad and allowed to grow for 4 weeks. (A) Representative western blot and quantification of plasma FN (pFN) in normal, non-tumor bearing mice and in 4T1 tumor bearing mice. A representative total protein (TP) band is shown as a loading control. n=5 per group (B-C) Representative western blot and quantification of soluble FN (sFN) and insoluble FN (iFN) in multiple tissues of normal and 4T1 tumor bearing mice. The term "gland and tumor" refers to the mammary gland and mammary tumor. ****P<0.0001, n=3 per group

PEG-FUD treatment reduced 4T1 tumor growth and decreased intratumoral FN levels

Previously we have demonstrated that PEG-FUD targets and accumulates in 4T1 mammary tumors compared to other organs using multiple imaging modalities(36). To investigate the therapeutic efficacy of targeting FN in the TME, we treated 4T1 orthotopic mammary tumors with the FN-targeting peptide, PEG-FUD, as an anti-cancer agent. One-week after 4T1 cancer cell injection into the right 4th mammary fat pad, when the average tumor size reached ~50 mm^3, mice were subcutaneously injected with either vehicle control (Ctrl_PBS) or 12.5 mg/kg (in peptide equivalent) of PEG-FUD, PEG-mFUD or PEG-FmFUD every 48hr for a total of 10 doses (Fig 3A). The mFUD and FmFUD control peptides are mutated versions of WT FUD with 7 or 10 mutation sites, respectively (Supplemental Fig 1A). Our results showed that PEG-FUD treatment

322 slowed tumor growth after just 4 doses compared to the control groups. Similarly, at endpoint (10
323 doses) PEG-FUD significantly reduced tumor volume compared to Ctrl_PBS and PEG-FmFUD
324 (Fig 3B-C). The control peptide, PEG-mFUD, had a partial effect in reducing tumor growth, while
325 tumor growth in the PEG-FmFUD treated mice was similar to the vehicle, Ctrl_PBS-treated mice.
326 This was not surprising, as we previously showed that PEG-mFUD partially inhibits b-FUD
327 binding to FN at high concentrations *in vitro*(36), and the partial binding of PEG-mFUD to FN
328 might be explained by the remaining (non-mutated) binding sites for FN present in PEG-mFUD
329 (Supplemental Fig 1A). This is further supported by the result from the fully mutated control
330 peptide, PEG-FmFUD, which has additional mutations in FN binding sites and did not bind to FN
331 in enzyme-linked competitive binding assay, suggesting that the additional mutations reduced
332 binding to FN *in vitro* (Supplemental Fig 2A).
333 As PEG-FUD binds to the 70-kDa region of cellular and plasma FN, we evaluated the
334 pharmacological effect of PEG-FUD on both plasma and intratumoral FN. First, we evaluated
335 circulating FN in the plasma isolated from whole blood using western blot analysis. Results
336 showed no changes in pFN levels between Ctrl_PBS and peptide treatment groups (Fig 3D). To
337 detect FN in tumors, flash frozen tumor tissue was lysed into two separate fractions, DOC-soluble
338 fraction containing sFN and DOC-insoluble fraction containing assembled iFN(47). Again, we
339 quantified FN levels in each tumor lysate fraction by western blot. As expected, 10 doses of PEG-
340 FUD significantly reduced iFN while no changes in sFN were observed (Fig 3E-F). As mentioned
341 previously, the shift in tumor growth rate in response to PEG-FUD occurred early in the treatment
342 time course. Therefore, we evaluated a subset of tumors from the Ctrl_PBS and PEG-FUD groups
343 at an earlier treatment time point (after 6 doses). Total FN levels in these tumors were assessed by
344 immunofluorescence staining. After just 6 doses of PEG-FUD, image analysis demonstrated a

345 significant decrease in the levels of total FN as quantified by mean fluorescent intensity per field

346 of view (Fig 3G-H).

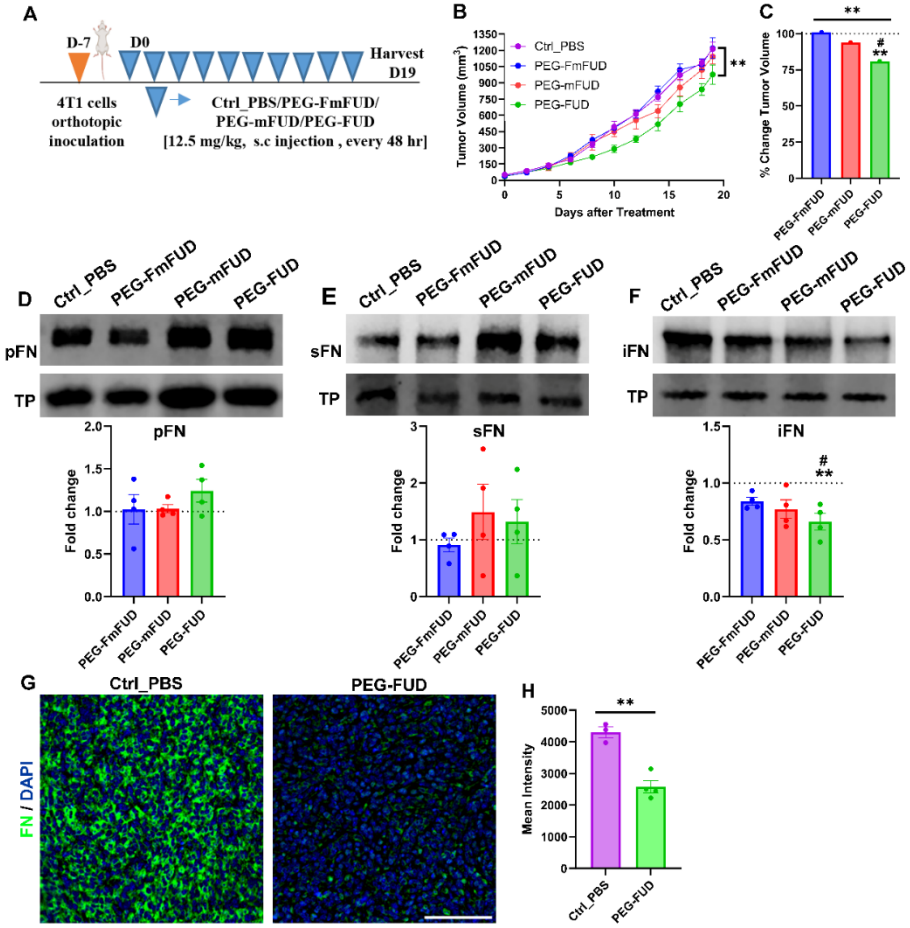

Figure 3: **PEG-FUD significantly reduced 4T1 tumor growth and FN in the TME** (A) Experimental design for therapeutic treatment. 9-week-old, female BALB/c mice were injected with 2×10^5 4T1 cells into the 4th mammary fat pad. Mice were subcutaneously (s.c) treated with vehicle control (Ctrl_PBS), PEG-FmFUD, PEG-mFUD, or PEG-FUD (10 doses of 12.5 mg/kg peptide) when tumors reached ~50 mm^3. (B) 4T1 tumor growth post Ctrl_PBS & peptide treatments. **P<0.005, n=4 per group. (C). % Change in 4T1 tumor volume from Ctrl_PBS to mice treated with PEG-FmFUD, PEG-mFUD, or PEG-FUD. # indicates significant fold change relative to significance from vehicle control (Ctrl_PBS). **P<0.005, n=4 per group. (D-F) Representative western blots and quantification of pFN, sFN, and iFN post Ctrl_PBS and peptide treatments. A representative total protein (TP) band is shown as a loading control. The graphs represent normalized band intensities to Ctrl_PBS treatment. # indicates significance from vehicle control (Ctrl_PBS) **P<0.005, n=4 per group (G-H) Immunofluorescence staining and quantification of FN in 4T1 tumors from Ctrl_PBS and PEG-FUD treated mice (6 doses of 12.5 mg/kg peptide). Scale bar = 100 µm. **P<0.005, n=3-4 per group.

347 FN is known to function as a provisional matrix for the deposition and structural organization of
348 additional fibrotic matrix proteins(24). Thus, the reduction in iFN levels in PEG-FUD treated
349 tumors led us to investigate potential changes in other peritumoral ECM proteins. Furthermore,
350 previous *in vivo* studies using FUD as an anti-fibrotic agent in other fibrotic diseases demonstrated
351 that FUD not only blocked FN assembly, but the treatment was accompanied by a reduction in
352 collagen deposition(31,34). To assess alterations in other ECM proteins in the 4T1 TME post-
353 PEG-FUD treatment, we probed tumor lysates for FN-interacting matrix proteins that we and
354 others have identified in the 4T1 tumor model(48–50). We investigated the levels of collagen
355 (COL1A1), tenascin-C (TNC) and periostin (POSTN) in the DOC-insoluble fraction of tumor
356 lysates by western blot. Surprisingly, our findings showed no significant changes in COL1A1,
357 TNC or POSTN (Supplemental Fig 3A-C). While the protein levels of COL1A1 remained
358 unchanged with PEG-FUD treatment, the possibility remained that collagen fiber architecture may
359 be altered due to the reduction in assembled FN. To evaluate collagen fiber architecture, we stained
360 sections with PSR and conducted second harmonic generation imaging of collagen on thick tumor
361 sections. Interestingly, PEG-FUD treatment did not alter collagen fiber area, nor did we observe
362 any apparent difference in fiber architecture in any of the treatment groups (Supplemental Fig 3D-
363 E). One possibility for this result may be due to the reduced, but not eliminated, level of iFN,
364 which allows for the residual FN fibrils to act as a template for collagen and other ECM deposition
365 in the TME.
366

367 **No significant toxicities were detected in PEG-FUD treated mice**

368 Drug-induced toxicity is a major concern in developing new treatments for breast cancer patients.
369 To validate the safe use of PEG-FUD as a therapeutic agent, we conducted a series of standard

toxicity and histologic assessments. No significant body weight changes or signs of distress were observed in mice within Ctrl_PBS or peptide treatment groups (Fig 4A). The spleen weights of control and peptide treated mice were not significantly different (Fig 4B). CBC analysis indicated no changes in white blood cells (WBC), lymphocytes (LYM), monocytes (MON), or neutrophils (NEU) (Fig 4C). Additionally, platelet levels were noted to be higher with PEG-FUD treatment although not statistically significant from control groups (Fig 4D). The platelet count after PEG-FUD treatment remained within the typical range of platelet counts reported in other studies utilizing BALB/c mice(51,52). Histopathologic analysis of kidneys identified mild to moderate intracytoplasmic vacuolation within cortical tubular epithelial cells in all peptide treatment groups. This vacuolar change was not observed in the vehicle treated, Ctrl_PBS group (Supplemental Fig 4A). Prior reports show that PEG-linked proteins can induce renal tubular vacuolation at high dose or repetitive low doses, yet modifications were not linked to any changes in clinical pathology or functional indicators(53). Histopathologic analysis of liver showed mild extramedullary hematopoiesis (EMH) in both Ctrl_PBS and peptide treatment groups, with no noted difference in abundance between groups, suggesting the findings may be due to the 4T1 tumor model rather than treatment (Supplemental Fig 4B).

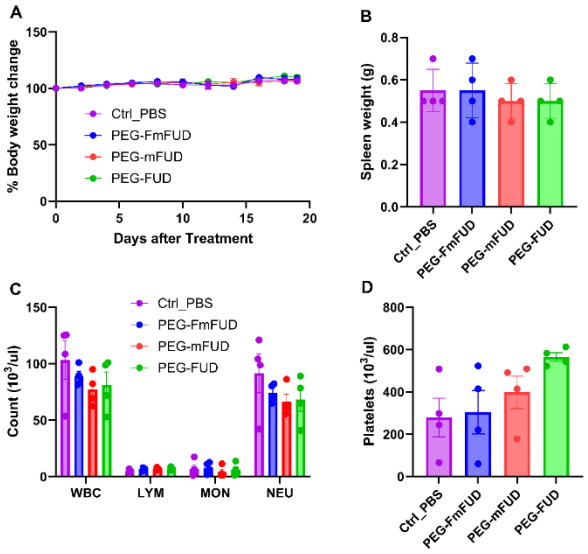

Figure 4: **No changes in toxicity profile post PEG-FUD treatment.** 2×10^5 4T1 tumor cells were injected into the 4th mammary fat pad and allowed to grow to 50 mm^3. Then animals were administered vehicle control (Ctrl_PBS) or 10 peptide treatments via subcutaneous injection every 48 hr. (A) Time course of body weight measurements collected at every treatment period. (B) Quantification of spleen weight measurements at the end of treatment. (C) Complete blood count analysis of white blood cells (WBC), lymphocytes (LYM), monocytes (MON), or neutrophils (NEU) at therapeutic end point. (D) Platelet levels post Ctrl_PBS and peptide treatments. n=4 per group

386

387 **PEG-FUD treatment did not affect cell survival or proliferation signaling**

388 FN is known to initiate signaling through integrin adhesion to activate AKT-mediated cell survival
389 pathways and cell proliferation via the MAPK/ERK pathway. Changes in one or both of these
390 pathways could play a role in the observed reduction in tumor size in PEG-FUD-treated mice. To
391 examine the effect of blocking FN assembly by PEG-FUD, we quantified cell survival signaling
392 by assessing total and phosphorylated AKT (p-AKT) levels in tumor lysates. Surprisingly, no
393 changes were observed in total AKT or activated p-AKT (Fig 5A). Next, we assessed ERK-
394 regulated cell proliferation by quantifying total and phosphorylated ERK (p-ERK). Similar to our
395 results with AKT activity, we found no changes in ERK activation in response to PEG-FUD
396 treatment (Fig 5B). Additionally, we examined two well-known cell proliferation markers, PCNA
397 in tumor lysates after 10 doses of peptide treatment and the area of Ki67+ cells after 6 dose of
398 peptide treatment, using western blotting and immunofluorescence, respectively. Consistent with
399 the above findings, we did not detect a change in either marker of cell proliferation in response to
400 PEG-FUD treatment compared to control groups (Fig 5C-E). Although these findings contradict
401 previous research showing that inhibiting FN decreased proliferation(28,30,31), this may be
402 explained by a difference in orthotopic tumor models or differences in growth factors present in
403 the TME of 4T1 tumors that could maintain proliferation signaling.

404

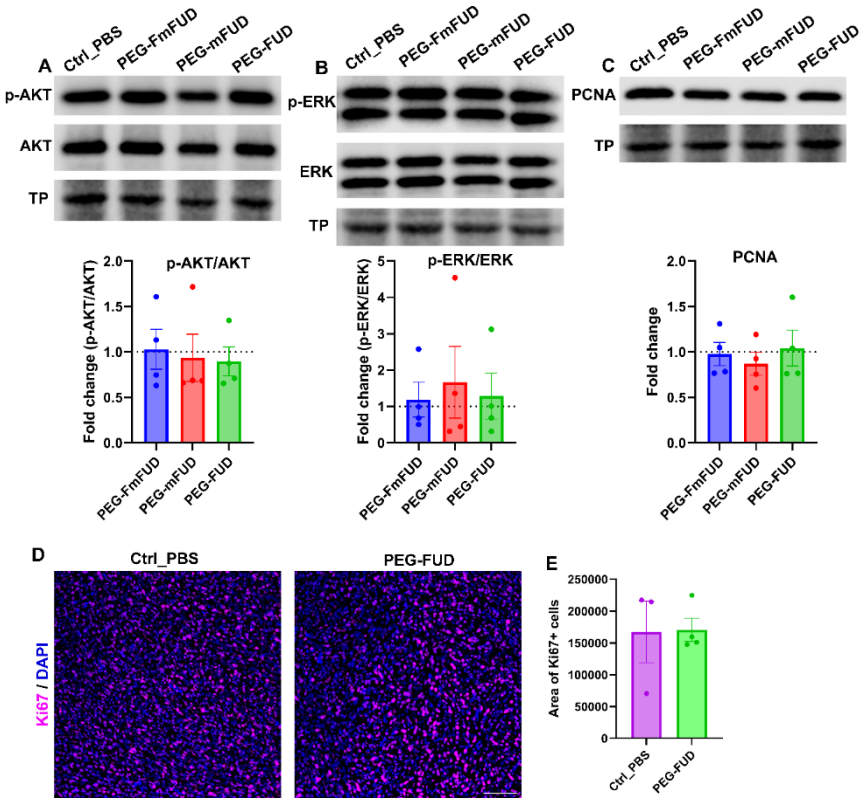

Figure 5: **No changes in cell survival / proliferation signaling post PEG-FUD treatment.** (A-C) Representative western blots and quantification of proliferation markers AKT, ERK and PCNA post vehicle control (Ctrl_PBS) and peptide treatments (10 doses of 12.5 mg/kg peptide). A representative total protein (TP) band is shown as a loading control. The graphs represent normalized band intensities to Ctrl_PBS treatment. (D) Representative immunofluorescent images stained for proliferation marker Ki67 post Ctrl_PBS and PEG-FUD treatment (6 doses of 12.5 mg/kg peptide). (E) Quantification of Ki67+ area from D.

Treatment with PEG-FUD reduced α5 integrin and FAK protein expression and promoted caspase-3 mediated cell death

Next, we sought to interrogate FN-mediated focal adhesions and downstream apoptotic signaling as part of the mechanism by which PEG-FUD therapy inhibits tumor growth. Integrin α5β1 is the primary receptor for FN that binds sFN and initiates the assembly of FN into a fibrillar matrix(54). In addition, the binding of integrins to FN activates intracellular signaling pathways downstream of focal adhesions(55). To determine whether adhesion-mediated signaling is disrupted in response

413 to PEG-FUD, we quantified the level of α5 and β1 integrins by western blot analysis. PEG-FUD
414 treatment resulted in a significant reduction in the tumor levels of integrin α5 (Fig 6A). In contrast,
415 PEG-FUD therapy did not affect β1 integrin (Fig 6B). β1 integrins form complexes with multiple
416 alpha integrins subunits to bind several ECM proteins found in the TME(56). Thus, the lack of β1
417 integrin specificity for FN is one possible rationale for the modulation of α5, but not β1 integrin,
418 in response to PEG-FUD treatment. Due to the reduction in iFN and α5 integrin levels, we next
419 evaluated the effect of PEG-FUD on the focal adhesion signaling through focal adhesion kinase
420 (FAK). FAK is a master regulator of cell adhesion signaling upon integrin activation and
421 clustering(57). Strikingly, we observed a significant reduction in total FAK protein levels in PEG-
422 FUD treated tumors compared to controls (Fig 6C). Taken together, these findings indicate that
423 inhibiting FN assembly with PEG-FUD alters FAK-dependent integrin-mediated cell adhesion.
424 In the literature, FN knockdown, blockade of FN receptor integrin α5β1, and alterations in FAK
425 have been shown to induce anoikis, a type of programmed cell death that results from a loss of
426 cell-ECM attachment(58,59). To investigate the effect of FN inhibition by PEG-FUD in mediating
427 cell death, we probed for cell death markers at both early and late treatment time points (6 or 10
428 doses of PEG-FUD). We confirmed the induction of cell death by PEG-FUD by a statistically
429 significant increase in cleaved caspase-3 levels from whole tumor lysates collected from mice that
430 received 10 doses of PEG-FUD compared to control-treated tumor groups (Fig 6D). Tumors
431 harvested from mice that received 6 doses of PEG-FUD showed a qualitative increase in the
432 presence of tumor necrosis identified in H&E stained sections (Fig 6E). Additionally,
433 representative serial sections from each treatment group were assessed by TUNEL assay. We
434 identified large TUNEL positive regions at the core of PEG-FUD treated tumors that are not

435 observed in the vehicle control (Ctrl_PBS) treated tumors (Fig 6F). Altogether, these results

436 suggest that PEG-FUD induced cell death by inhibiting FN-integrin-mediated cell adhesion.

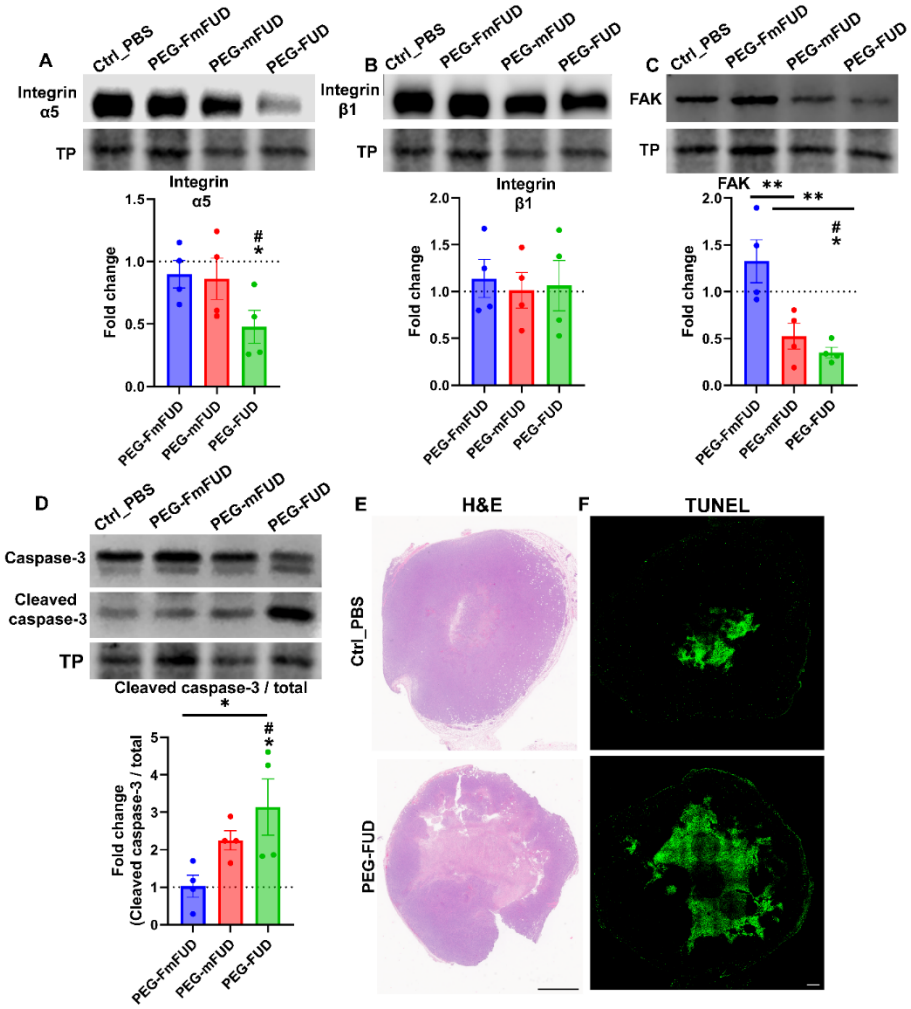

Figure 6: **PEG-FUD alters integrin mediated adhesion signaling and cell death.** (A-D) Representative western blots and quantification of Integrin α5, Integrin β1, FAK, caspase-3 and cleaved caspase-3 from 4T1 tumor lysates treated with vehicle control (Ctrl_PBS) and peptides (10 doses of 12.5 mg/kg peptide). A representative total protein (TP) band is shown as a loading control. The graphs represent normalized band intensities to Ctrl_PBS treatment. # indicates significant fold change relative to significance from vehicle control (Ctrl_PBS). *P<0.05, **P<0.005, n=4 per group (E) Representative images of H&E staining and TUNEL staining of 4T1 tumor sections from mice treated with Ctrl_PBS and PEG-FUD (6 doses of 12.5 mg/kg peptide). H&E Scale bar = 100 µm; TUNEL Scale bar = 500 µm.

437

438 **PEG-FUD primes the mammary TME for enhanced anti-tumor efficacy of doxorubicin**

439 The identification of PEG-FUD-mediated tumor cell death led us to hypothesize that PEG-FUD
440 not only has intrinsic anti-cancer potential but may also synergistically improve the tumor response
441 to chemotherapy. Others have demonstrated that the overexpression of FAK, which is identified in
442 multiple tumors, plays a critical role in suppressing tumor cell death and facilitating resistance to
443 Dox(60,61). Based on these findings and our evidence for PEG-FUD to robustly inhibit FAK
444 protein levels in the 4T1 TME, we tested the ability of PEG-FUD pre-treatment to improve the
445 response of a commonly used chemotherapeutic drug, Dox, in the 4T1 tumor model. 4T1
446 orthotropic tumors were established similarly to the PEG-FUD monotherapy approach with
447 treatment starting when the average tumor size reached ~50 mm^3. Mice were randomized into
448 treatment groups and subcutaneously injected with either vehicle control (Ctrl_PBS) or 12.5 mg/kg
449 (in peptide equivalent) of PEG-FUD or PEG-FmFUD every 48 hr for 4 doses. At the 4-dose
450 timepoint (when a shift in tumor growth was noted, Fig 3B), we initiated intraperitoneal
451 administration of Dox at 5mg/kg every 72 hr with continued peptide treatment (experimental
452 design outlined in Fig 7A). Combinatorial treatment of PEG-FUD and Dox resulted in a significant
453 reduction in tumor growth by ~60% to vehicle control and by an additional ~30% to Dox alone,
454 demonstrating that PEG-FUD co-treatment increased the efficacy of Dox therapy in the 4T1 TNBC
455 model (Fig 7B-C). Mice treated with Dox exhibited loss of body and spleen weight due to the well-
456 known systemic toxicity of Dox, but no additive effect was detected with co-treatment with PEG-
457 FUD (Fig 7D-E). These findings provide evidence that reducing FN with PEG-FUD improves
458 chemotherapeutic response.
459
460

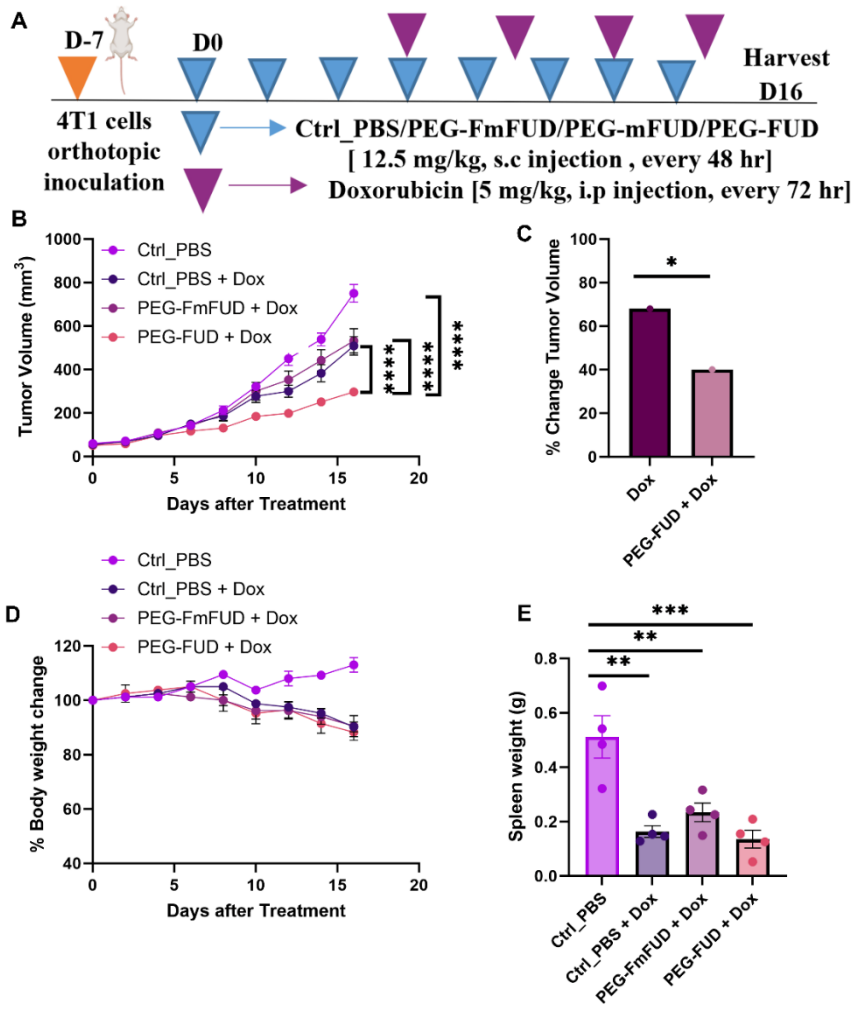

Figure 7: **PEG-FUD combined with Doxorubicin resulted in enhanced efficacy without additional toxicity.** (A) Experimental design for therapeutic treatment. 9-week-old, female BALB/c mice were injected with 2×10^5 4T1 cells into the 4th mammary fat pad. Mice were subcutaneously (s.c) treated with 4 doses of vehicle control (Ctrl_PBS), PEG-FmFUD, or PEG-FUD at 12.5 mg/kg every 48 hrs once tumors reached ~ 50 mm^3. Upon the 4th dose of PEG-FUD, Doxorubicin (Dox) was administered intraperitoneally (i.p) at 5mg/kg every 72 hr with continued peptide treatment until day 16 post 4T1 tumor cell inoculation. (B) 4T1 tumor growth post Ctrl_PBS and combined treatments. ****P<0.0001, n=4 per group. (C). % Change in 4T1 tumor volume from Ctrl_PBS to mice treated with Dox and PEG-FUD + Dox. *P<0.05, n=4 per group. (D) Time course of body weight measurements collected at every treatment period post vehicle control (Ctrl_PBS), Dox and peptide + Dox combination treatments. (E) Quantification of spleen weights post Ctrl_PBS, Dox and peptide combination treatments at the end of treatment period. **P<0.005, ***P<0.001, n=4 mice per group.

463 **Discussion**

464 In this study, we investigated the anti-cancer effects of targeting FN matrix assembly in the TME
465 using PEG-FUD. Several FN-targeting strategies have been developed and demonstrated promise
466 in the diagnosis, therapy, and image-guided interventions of a variety of malignancies(62). For
467 example, antibodies that detect the EDA domain of cellular FN have shown promise for solid
468 tumor diagnostics(63). Additional studies expanded on the utility of targeting FN by developing
469 antibody-drug conjugates using an EDA-antibody with anti-IL-2(64), EDA expressing CAR-T
470 cells(65), or developing fibrin-FN binding peptides conjugated with Dox(66) for enhanced
471 therapeutic efficacy and reduced systemic toxicities. Some of these approaches made it to early-
472 phase human trials, however, they have yet to be FDA-approved for the clinical treatment of breast
473 cancer. Thus, developing new therapeutic approaches to target FN in the TME is both timely and
474 promising.

475 Here, we take advantage of targeting FN with PEG-FUD. PEG-FUD binds with high affinity to
476 the 70-kDa N-terminus and inhibits the assembly of all sources of FN (cellular and plasma derived
477 FN). This is essential since both sources of FN can be deposited in the tumor matrix(67,68). We
478 previously reported that PEG-FUD accumulates and is maintained in 4T1 tumors for prolonged
479 periods compared to FUD alone(36). Our current *in vitro* data demonstrate that PEG-FUD
480 successfully inhibited the assembly of endogenous FN assembled by mammary CAFs (Fig 1). In
481 addition, we demonstrated that PEG-FUD is effective when given in therapeutic doses to reduce
482 the assembly of tumor FN (decreased iFN levels) and to suppress 4T1 tumor growth (Fig 3).
483 Therefore, like prior studies we confirmed that the PEGylation of the FUD peptide retained the
484 ability to block FN assembly(33,34,36). Together these data demonstrate the utility of PEG-FUD
485 not only for tumor diagnostics but also as an anti-breast cancer therapeutic.

486 Mechanistically we determined that PEG-FUD treatment significantly reduced levels of α5
487 integrin, a major adhesion receptor for FN. Integrin binding to FN mediates intracellular signaling
488 to regulate cellular processes such as cell growth, proliferation, and migration(69–71). Despite the
489 significant reduction in α5 integrin and FAK, we did not observe differences in proliferation or
490 survival signaling through ERK or AKT, respectively. This result contradicts previous observations
491 that FUD/puR4 peptide decreased ERK phosphorylation without affecting FAK or AKT
492 phosphorylation(31). However, the difference between our findings and those of Ghura et al. may
493 be explained by differences in model systems (immune competent vs immune compromised),
494 treatment conditions (PEG-FUD vs FUD), and identification of altered signaling pathways (within
495 tumors vs in cell culture). Furthermore, ERK and AKT activation can occur independent of FN-
496 FAK mediated signaling. In support of this hypothesis, a study utilizing an integrin antagonist 1a-
497 RGD in glioblastoma cells showed that by inhibiting cell adhesion, FAK activation decreased
498 without altering ERK and AKT-dependent pathways(72). It is also plausible that the reduction in
499 iFN could release growth hormones normally sequestered in the matrix that become available to
500 bind and activate pathways downstream of growth factor receptors(73–76).

501 In our study, the loss of α5 and FAK in the TME in response to PEG-FUD is notable. While we do
502 not know the temporal sequence of α5 integrin vs FAK down-regulation, the functional inhibition
503 of α5β1 integrin activation has been shown to reduce total FAK expression and protein levels(77).
504 Others have also demonstrated that caspase-mediated FAK cleavage (degradation of FAK) causes
505 focal adhesion complexes to disassemble(78), suggesting the activation of caspase signaling could
506 reduce levels of FAK and α5 integrin. Importantly, the disassembly of focal adhesions down stream
507 of caspase activation interferes with integrin-mediated survival signaling, thereby propagating the
508 cell death program(78). In line with these studies, we identified an increase in TUNEL-positive

509 staining and caspase-3 mediated cell death in PEG-FUD-treated tumors. Multiple studies have
510 shown that integrin adhesion to FN can induce anoikis resistance and reduce apoptosis(58,79).
511 Moreover, FAK itself has been identified to play a critical role in suppressing cell death(80–83).
512 FAK has been shown to directly bind to the death domain of receptor-interacting protein (RIP) to
513 suppress apoptosis(61). RIP provides proapoptotic signals that are suppressed upon binding to
514 FAK, thus blocking the FAK-RIP interaction or reducing total FAK levels shifts cells toward
515 caspase-mediated cell death. Taken together, our findings suggest that PEG-FUD effectively
516 blocked FN assembly within the TME resulting in decreased α5 integrin and FAK levels, leading
517 to apoptosis via the activation of caspase-3 cleavage. This results in an overall reduction in tumor
518 growth, demonstrating PEG-FUD as an effective single agent therapy to target pre-clinical breast
519 cancer.

520 Our characterization of the tumor response to PEG-FUD also demonstrates the promise of
521 targeting FN to improve standard-of-care cancer therapies. For many solid tumors, including
522 TNBC, the first-line treatment is chemotherapy. However, the ECM of solid breast tumors
523 activates mechanisms of drug resistance that significantly impede clinical therapies(84–86). Other
524 pre-clinical mammary tumor studies have shown that Pirfenidone, an FDA approved antifibrotic
525 drug for idiopathic pulmonary fibrosis, normalizes the tumor ECM for enhanced chemotherapy
526 response, demonstrating the value of ECM normalization(87). This study focused on the action of
527 pirfenidone to block TGF-b signaling and downstream ECM deposition, which led to increased
528 drug penetration. Our data suggest that the anti-fibrotic impact of PEG-FUD not only reduces iFN
529 within tumors but also alleviates ECM-mediated mechanisms of drug resistance through the
530 reduction of FAK. In line with our findings, van Nimwegen et al. illuminated a mechanism by
531 which adhesion-mediated stress fiber formation and FAK activation suppressed Dox-induced

532 apoptosis(60). Based on these results, we hypothesized that by reducing tumoral FN and inhibiting
533 α5 integrin and FAK, PEG-FUD sufficiently primed the TME for improved chemotherapy
534 response. Indeed, when 4T1 tumors were primed with PEG-FUD followed by combined treatment
535 with Dox + PEG-FUD we quantified a 60% decrease in tumor growth compared to vehicle control
536 and 30% compared to Dox monotherapy. Notably, combinatorial treatment of PEG-FUD and Dox
537 did not increase the systemic toxicity of Dox (Fig 7). Thus, PEG-FUD therapy is an effective
538 strategy to improve the efficacy of standard-of-care chemotherapy in 4T1 TNBC model.
539

540 **Conclusion**

541 In summary, we have demonstrated the efficacy of PEG-FUD to target FN in 4T1 triple-negative
542 tumors and improve response to standard chemotherapy. We have characterized changes in the
543 TME in response to PEG-FUD treatment and identified a mechanism where the reduction in iFN
544 leads to a significant decrease in α5 integrin and FAK levels. Further, these changes in cell
545 adhesion increased tumor cell death and blocked tumor growth. Strikingly, the tumor response to
546 PEG-FUD therapy was sufficient to prime the TME into a non-tumor-supporting
547 microenvironment and significantly enhance the efficacy of Dox therapy. As we previously
548 demonstrated PEG-FUD can also target the metastatic microenvironment(36), our future studies
549 will explore PEG-FUD as an effective treatment for metastatic breast cancer.
550
551
552
553

554 # References

555 1. Conklin MW, Keely PJ. Why the stroma matters in breast cancer: Insights into breast
556 cancer patient outcomes through the examination of stromal biomarkers. Cell Adh
557 Migr [Internet]. 2012 [cited 2024 Jul 14];6(3):249–60. Available from:
558 https://www.tandfonline.com/action/journalInformation?journalCode=kcam20

559 2. Oskarsson T. Extracellular matrix components in breast cancer progression and
560 metastasis. Breast [Internet]. 2013 Aug 1 [cited 2024 Jul 14];22 Suppl 2(S2). Available
561 from: https://pubmed.ncbi.nlm.nih.gov/24074795/

562 3. Fertal SA, Poterala JE, Ponik SM, Wisinski KB. Stromal Characteristics and Impact on
563 New Therapies for Metastatic Triple-Negative Breast Cancer. Cancers (Basel)
564 [Internet]. 2022 Mar 1 [cited 2024 Jul 14];14(5). Available from:
565 https://pubmed.ncbi.nlm.nih.gov/35267548/

566 4. Anttila MA, Tammi RH, Tammi MI, Syrjänen KJ, Saarikoski S V, Kosma VM. High Levels
567 of Stromal Hyaluronan Predict Poor Disease Outcome in Epithelial Ovarian Cancer 1.
568 Cancer Res [Internet]. 2000 [cited 2024 Jun 30];60:150–5. Available from:
569 http://aacrjournals.org/cancerres/article-pdf/60/1/150/3241293/ch010000150p.pdf

570 5. Parker AL, Bowman E, Zingone A, Ryan BM, Cooper WA, Kohonen-Corish M, et al.
571 Extracellular matrix profiles determine risk and prognosis of the squamous cell
572 carcinoma subtype of non-small cell lung carcinoma. Genome Medicine 2022 14:1
573 [Internet]. 2022 Nov 21 [cited 2024 Jun 30];14(1):1–29. Available from:
574 https://genomemedicine.biomedcentral.com/articles/10.1186/s13073-022-01127-6

575 6. Yuzhalin AE, Urbonas T, Silva MA, Muschel RJ, Gordon-Weeks AN. A core matrisome
576 gene signature predicts cancer outcome. Nature Publishing Group [Internet]. 2018
577 [cited 2024 Jun 30];118. Available from: http://matrisomeproject.mit.edu/

578 7. Bae YK, Kim A, Kim MK, Choi JE, Kang SH, Lee SJ. Fibronectin expression in
579 carcinoma cells correlates with tumor aggressiveness and poor clinical outcome in
580 patients with invasive breast cancer. Hum Pathol. 2013 Oct 1;44(10):2028–37.

581 8. Conklin MW, Eickhoff JC, Riching KM, Pehlke CA, Eliceiri KW, Provenzano PP, et al.
582 Aligned Collagen Is a Prognostic Signature for Survival in Human Breast Carcinoma.
583 Am J Pathol [Internet]. 2011 [cited 2022 Mar 5];178(3):1221. Available from:
584 /pmc/articles/PMC3070581/

585 9. Esbona K, Yi Y, Saha S, Yu M, Van Doorn RR, Conklin MW, et al. The Presence of
586 Cyclooxygenase 2, Tumor-Associated Macrophages, and Collagen Alignment as

Prognostic Markers for Invasive Breast Carcinoma Patients. American Journal of Pathology [Internet]. 2018 Mar 1 [cited 2024 Jun 29];188(3):559–73. Available from: http://ajp.amjpathol.org/article/S0002944017302833/fulltext

10. Liu J, Liao S, Diop-Frimpong B, Chen W, Goel S, Naxerova K, et al. TGF-β blockade improves the distribution and efficacy of therapeutics in breast carcinoma by normalizing the tumor stroma. Proc Natl Acad Sci U S A [Internet]. 2012 Oct 9 [cited 2024 Jun 16];109(41):16618–23. Available from: www.pnas.org/cgi/doi/10.1073/pnas.1117610109

11. Vandenbroucke RE, Libert C. Is there new hope for therapeutic matrix metalloproteinase inhibition? Nature Publishing Group [Internet]. 2014 [cited 2024 Jun 16]; Available from: www.nature.com/reviews/drugdisc

12. Mariathasan S, Turley SJ, Nickles D, Castiglioni A, yuen K, Wang yulei, et al. TGFβ attenuates tumour response to PD-L1 blockade by contributing to exclusion of T cells. 2018;

13. Coulson R, Liew SH, Connelly AA, Yee NS, Deb S, Kumar B, et al. The angiotensin receptor blocker, Losartan, inhibits mammary tumor development and progression to invasive carcinoma. Oncotarget [Internet]. 2017 [cited 2024 Jun 16];8(12):18640–56. Available from: www.impactjournals.com/oncotarget/

14. Sparano JA, Bernardo P, Stephenson P, Gradishar WJ, Ingle JN, Zucker S, et al. Randomized Phase III Trial of Marimastat Versus Placebo in Patients With Metastatic Breast Cancer Who Have Responding or Stable Disease After First-Line Chemotherapy: Eastern Cooperative Oncology Group Trial E2196. J Clin Oncol [Internet]. 2004 [cited 2024 Jun 16];22:4683–90. Available from: www.jco.org

15. Keiser HR, Sjoerdsma A. Studies on beta-aminopropionitrile in patients with scleroderma. Clinical Pharmacology andTherapeutics. 1967;8(4):593–602.

16. Giaccone G, Bazhenova LA, Nemunaitis J, Tan M, Juhász E, Ramlau R, et al. A phase III study of belagenpumatucel-L, an allogeneic tumour cell vaccine, as maintenance therapy for non-small cell lung cancer. Eur J Cancer [Internet]. 2015 Nov 1 [cited 2024 Jun 16];51(16):2321–9. Available from: http://www.ejcancer.com/article/S0959804915007418/fulltext

17. Sleeboom JJF, van Tienderen GS, Schenke-Layland K, van der Laan LJW, Khalil AA, Verstegen MMA. The extracellular matrix as hallmark of cancer and metastasis: From biomechanics to therapeutic targets. Sci Transl Med [Internet]. 2024 Jan 3 [cited

2024 Nov 3];16(728). Available from: https://www.science.org/doi/10.1126/scitranslmed.adg3840

18. Tomko LA, Hill RC, Barrett A, Szulczewski JM, Conklin MW, Eliceiri KW, et al. Targeted matrisome analysis identifies thrombospondin-2 and tenascin-C in aligned collagen stroma from invasive breast carcinoma. Scientific Reports 2018 8:1 [Internet]. 2018 Aug 28 [cited 2022 Mar 5];8(1):1–11. Available from: https://www.nature.com/articles/s41598-018-31126-w

19. Spada S, Tocci A, Di Modugno F, Nisticò P. Fibronectin as a multiregulatory molecule crucial in tumor matrisome: from structural and functional features to clinical practice in oncology. Journal of Experimental & Clinical Cancer Research 2021 40:1 [Internet]. 2021 Mar 17 [cited 2024 Jul 14];40(1):1–14. Available from: https://jeccr.biomedcentral.com/articles/10.1186/s13046-021-01908-8

20. Hebert JD, Myers SA, Naba A, Abbruzzese G, Lamar JM, Carr SA, et al. Proteomic profiling of the ECM of xenograft breast cancer metastases in different organs reveals distinct metastatic niches. Cancer Res [Internet]. 2020 Apr 1 [cited 2024 Nov 3];80(7):1475–85. Available from: /cancerres/article/80/7/1475/647712/Proteomic-Profiling-of-the-ECM-of-Xenograft-Breast

21. Hynes RO, Yamada KM. Fibronectins: Multifunctional Modular Glycoproteins. [cited 2024 May 13]; Available from: http://rupress.org/jcb/article-pdf/95/2/369/1641134/369.pdf

22. Wierzbicka-Patynowski I, Schwarzbauer JE. The ins and outs of fibronectin matrix assembly. J Cell Sci [Internet]. 2003 Aug 15 [cited 2024 May 13];116(16):3269–76. Available from: https://dx.doi.org/10.1242/jcs.00670

23. Mckeown-Longo PJ, Mosher DF. Interaction of the 70,000-mol-wt Amino-terminal Fragment of Fibronectin with the Matrix-assembly Receptor of Fibroblasts. [cited 2024 May 2]; Available from: http://rupress.org/jcb/article-pdf/100/2/364/1457627/364.pdf

24. Sottile J, Hocking DC. Fibronectin Polymerization Regulates the Composition and Stability of Extracellular Matrix Fibrils and Cell-Matrix Adhesions. Mol Biol Cell. 2002;13:3546–59.

25. Pankov R, Yamada KM. Fibronectin at a glance. J Cell Sci [Internet]. 2002 Oct 15 [cited 2024 Jul 14];115(20):3861–3. Available from: https://dx.doi.org/10.1242/jcs.00059

26. Wang K, Wu F, Seo BR, Fischbach C, Chen W, Hsu L, et al. Breast cancer cells alter the dynamics of stromal fibronectin-collagen interactions. Matrix Biol [Internet]. 2017 Jul 1 [cited 2024 Jul 15];60–61:86. Available from: /pmc/articles/PMC5293676/

27. Tomasini-Johansson BR, Kaufman NR, Ensenberger MG, Ozeri V, Hanski E, Mosher DF. A 49-Residue Peptide from Adhesin F1 of Streptococcus pyogenes Inhibits Fibronectin Matrix Assembly *. Journal of Biological Chemistry [Internet]. 2001 Jun 29 [cited 2022 Mar 19];276(26):23430–9. Available from: http://www.jbc.org/article/S0021925820783316/fulltext

28. Chiang HY, Korshunov VA, Serour A, Shi F, Sottile J. Fibronectin is an important regulator of flow-induced vascular remodeling. Arterioscler Thromb Vasc Biol [Internet]. 2009 Jul 1 [cited 2022 Mar 19];29(7):1074. Available from: /pmc/articles/PMC3091823/

29. Altrock E, Sens C, Wuerfel C, Vasel M, Kawelke N, Dooley S, et al. Inhibition of fibronectin deposition improves experimental liver fibrosis. J Hepatol [Internet]. 2015 Mar 1 [cited 2022 Mar 19];62(3):625–33. Available from: http://www.journal-of-hepatology.eu/article/S016882781400405X/fulltext

30. Valiente-Alandi I, Potter SJ, Salvador AM, Schafer AE, Schips T, Carrillo-Salinas F, et al. Inhibiting fibronectin attenuates fibrosis and improves cardiac function in a model of heart failure. Circulation [Internet]. 2018 [cited 2022 Mar 19];138(12):1236. Available from: /pmc/articles/PMC6186194/

31. Ghura H, Keimer M, von Au A, Hackl N, Klemis V, Nakchbandi IA. Inhibition of fibronectin accumulation suppresses TUMOR growth. Neoplasia (United States). 2021 Sep 1;23(9):837–50.

32. Lee HJ, Tomasini-Johansson BR, Gupta N, Kwon GS. Fibronectin-targeted FUD and PEGylated FUD peptides for fibrotic diseases. Journal of Controlled Release. 2023 Aug 1;360:69–81.

33. Zbyszynski P, Tomasini-Johansson BR, Peters DM, Kwon GS. Characterization of the PEGylated Functional Upstream Domain Peptide (PEG-FUD): a Potent Fibronectin Assembly Inhibitor with Potential as an Anti-Fibrotic Therapeutic. Pharm Res [Internet]. 2018 Jul 1 [cited 2022 Feb 5];35(7):126. Available from: /pmc/articles/PMC6186450/

34. Tomasini-Johansson BR, Zbyszynski PW, Toraason I, Peters DM, Kwon GS. PEGylated pUR4/FUD peptide inhibitor of fibronectin fibrillogenesis decreases fibrosis in murine Unilateral Ureteral Obstruction model of kidney disease. PLoS One [Internet].

2018 Oct 1 [cited 2022 May 7];13(10):e0205360. Available from: https://journals.plos.org/plosone/article?id=10.1371/journal.pone.0205360

35. Zbyszynski P, Toraason I, Repp L, Kwon GS. Probing the subcutaneous absorption of a PEGylated FUD peptide nanomedicine via in vivo fluorescence imaging. Nano Converg [Internet]. 2019 Dec 1 [cited 2022 Feb 9];6(1):1–15. Available from: https://nanoconvergencejournal.springeropen.com/articles/10.1186/s40580-019-0192-3

36. Lee HJ, Gari MK, Inman DR, Rosenkrans ZT, Burkel BM, Olson AP, et al. Multimodal imaging demonstrates enhanced tumor exposure of PEGylated FUD peptide in breast cancer. Journal of Controlled Release. 2022 Oct 1;350:284–97.

37. Maurer LM, Tomasini-Johansson BR, Ma W, Annis DS, Eickstaedt NL, Ensenberger MG, et al. Extended binding site on fibronectin for the functional upstream domain of protein F1 of Streptococcus pyogenes. J Biol Chem [Internet]. 2010 Dec 24 [cited 2024 Jul 9];285(52):41087–99. Available from: https://pubmed.ncbi.nlm.nih.gov/20947497/

38. Ma W, Ma H, Mosher DF. On-Off Kinetics of Engagement of FNI Modules of Soluble Fibronectin by β-Strand Addition. PLoS One [Internet]. 2015 Apr 28 [cited 2024 Jul 9];10(4). Available from: https://pubmed.ncbi.nlm.nih.gov/25919138/

39. Ishihara S, Inman DR, Li WJ, Ponik SM, Keely PJ. Tumor and Stem Cell Biology Mechano-Signal Transduction in Mesenchymal Stem Cells Induces Prosaposin Secretion to Drive the Proliferation of Breast Cancer Cells. [cited 2024 May 5]; Available from: http://cancerres.aacrjournals.org/

40. Tomayko MM, Reynolds CP. ancer hemotherapy and harmacology Determination of subcutaneous tumor size in athymic (nude) mice*. Cancer Chemother Pharmacol. 1989;24:148–54.

41. Attieh Y, Clark AG, Grass C, Richon S, Pocard M, Mariani P, et al. Cancer-associated fibroblasts lead tumor invasion through integrin-β3-dependent fibronectin assembly. J Cell Biol [Internet]. 2017 Nov 1 [cited 2024 Jun 17];216(11):3509–20. Available from: https://pubmed.ncbi.nlm.nih.gov/28931556/

42. Tomasini-Johansson BR, Zbyszynski PW, Toraason I, Peters DM, Kwon GS. PEGylated pUR4/FUD peptide inhibitor of fibronectin fibrillogenesis decreases fibrosis in murine Unilateral Ureteral Obstruction model of kidney disease. PLoS One [Internet]. 2018 Oct 1 [cited 2022 Mar 19];13(10):e0205360. Available from: https://journals.plos.org/plosone/article?id=10.1371/journal.pone.0205360

721 43. Bae YK, Kim A, Kim MK, Choi JE, Kang SH, Lee SJ. Fibronectin expression in
722 carcinoma cells correlates with tumor aggressiveness and poor clinical outcome in
723 patients with invasive breast cancer. Hum Pathol. 2013 Oct 1;44(10):2028–37.

724 44. Zhang XX, Luo JH, Wu LQ. FN1 overexpression is correlated with unfavorable
725 prognosis and immune infiltrates in breast cancer. Front Genet [Internet]. 2022 Aug
726 12 [cited 2024 May 13];13. Available from: /pmc/articles/PMC9417469/

727 45. Pulaski BA, Ostrand-Rosenberg S. Mouse 4T1 Breast Tumor Model. Curr Protoc
728 Immunol [Internet]. 2000 Oct 1 [cited 2024 May 6];39(1):20.2.1-20.2.16. Available
729 from: https://onlinelibrary.wiley.com/doi/full/10.1002/0471142735.im2002s39

730 46. Zhou Z, Qutaish M, Han Z, Schur RM, Liu Y, Wilson DL, et al. MRI detection of breast
731 cancer micrometastases with a fibronectin-targeting contrast agent. Nat Commun
732 [Internet]. 2015 Aug 12 [cited 2022 Mar 19];6. Available from:
733 /pmc/articles/PMC4557274/

734 47. McKeown Longo PJ, Mosher DF. Binding of plasma fibronectin to cell layers of human
735 skin fibroblasts. J Cell Biol [Internet]. 1983 Aug 8 [cited 2024 Jun 27];97(2):466.
736 Available from: /pmc/articles/PMC2112508/?report=abstract

737 48. Ishihara S, Inman DR, Li WJ, Ponik SM, Keely PJ. Mechano-signal transduction in
738 mesenchymal stem cells induces prosaposin secretion to drive the proliferation of
739 breast cancer cells.

740 49. O'Connell JT, Sugimoto H, Cooke VG, MacDonald BA, Mehta AI, LeBleu VS, et al.
741 VEGF-A and Tenascin-C produced by S100A4 + stromal cells are important for
742 metastatic colonization. Proc Natl Acad Sci U S A [Internet]. 2011 Oct 20 [cited 2024
743 Jun 17];108(38):16002–7. Available from:
744 www.pnas.org/cgi/doi/10.1073/pnas.1109493108

745 50. Kyutoku M, Taniyama Y, Katsuragi N, Shimizu H, Kunugiza Y, Iekushi K, et al. Role of
746 periostin in cancer progression and metastasis: Inhibition of breast cancer
747 progression and metastasis by anti-periostin antibody in a murine model. Int J Mol
748 Med [Internet]. 2011 Aug 1 [cited 2024 Jun 17];28(2):181–6. Available from:
749 http://www.spandidos-publications.com/10.3892/ijmm.2011.712/abstract

750 51. Wang C, Chen YG, Gao JL, Lyu GY, Su J, Zhang Q, et al. Low local blood perfusion,
751 high white blood cell and high platelet count are associated with primary tumor
752 growth and lung metastasis in a 4T1 mouse breast cancer metastasis model. Oncol
753 Lett [Internet]. 2015 Aug 1 [cited 2024 May 13];10(2):754–60. Available from:
754 http://www.spandidos-publications.com/10.3892/ol.2015.3304/abstract

52. Barrios M, Rodríguez-Acosta A, Gil A, Salazar AM, Taylor P, Sánchez EE, et al. Comparative hemostatic parameters in BALB/c, C57BL/6 and C3H/He mice. Thromb Res. 2009 Jul 1;124(3):338–43.

53. Bendele A, Seely J, Richey C, Sennello G, Shopp G. Short Communication: Renal Tubular Vacuolation in Animals Treated with Polyethylene-Glycol-Conjugated Proteins. 1998 [cited 2024 May 12]; Available from: https://academic.oup.com/toxsci/article/42/2/152/1685757

54. Singh P, Carraher C, Schwarzbauer JE. Assembly of Fibronectin Extracellular Matrix. Annu Rev Cell Dev Biol [Internet]. 2010 Nov 10 [cited 2024 May 13];26:397. Available from: /pmc/articles/PMC3628685/

55. Harburger DS, Calderwood DA. Integrin signalling at a glance. J Cell Sci [Internet]. 2009 Jan 1 [cited 2024 May 13];122(2):159. Available from: /pmc/articles/PMC2714413/

56. Sun L, Guo S, Xie Y, Yao Y. The characteristics and the multiple functions of integrin β1 in human cancers. J Transl Med [Internet]. 2023 [cited 2024 Jun 18];21:787. Available from: https://doi.org/10.1186/s12967-023-04696-1

57. Michael KE, Dumbauld DW, Burns KL, Hanks SK, García AJ. Focal adhesion kinase modulates cell adhesion strengthening via integrin activation. Mol Biol Cell [Internet]. 2009 May 1 [cited 2024 Jun 18];20(9):2508–19. Available from: https://www.molbiolcell.org/doi/10.1091/mbc.e08-01-0076

58. Han H jun, Sung JY, Kim SH, Yun UJ, Kim H, Jang EJ, et al. Fibronectin regulates anoikis resistance via cell aggregate formation. Cancer Lett. 2021 Jun 28;508:59–72.

59. Haun F, Neumann S, Peintner L, Wieland K, Habicht J, Schwan C, et al. Identification of a novel anoikis signalling pathway using the fungal virulence factor gliotoxin. [cited 2024 Jul 15]; Available from: www.nature.com/naturecommunications

60. Van Nimwegen MJ, Huigsloot M, Camier A, Tijdens IB, Van De Water B. Focal Adhesion Kinase and Protein Kinase B Cooperate to Suppress Doxorubicin-Induced Apoptosis of Breast Tumor Cells. 2006 [cited 2024 Jul 14]; Available from: http://molpharm.aspetjournals.org.

61. Kurenova E, Xu LH, Yang X, Albert S. Baldwin Jr, Craven RJ, Hanks SK, et al. Focal Adhesion Kinase Suppresses Apoptosis by Binding to the Death Domain of Receptor-Interacting Protein. Mol Cell Biol [Internet]. 2004 May 1 [cited 2024 Jul 14];24(10):4361. Available from: /pmc/articles/PMC400455/

62. Han Z, Lu ZR. Targeting Fibronectin for Cancer Imaging and Therapy. Journal of materials chemistry B, Materials for biology and medicine [Internet]. 2017 [cited 2022 May 7];5(4):639. Available from: /pmc/articles/PMC5733799/

63. Kumra H, Reinhardt DP. Fibronectin-targeted drug delivery in cancer. Adv Drug Deliv Rev. 2016 Feb 1;97:101–10.

64. Frey K, Schliemann C, Schwager K, Giavazzi R, Johannsen M, Neri D. The immunocytokine F8-IL2 improves the therapeutic performance of sunitinib in a mouse model of renal cell carcinoma. Journal of Urology. 2010 Dec;184(6):2540–8.

65. Martín-Otal C, Lasarte-Cia A, Serrano D, Casares N, Conde E, Navarro F, et al. Targeting the extra domain A of fibronectin for cancer therapy with CAR-T cells. J Immunother Cancer [Internet]. 2022 Aug 2 [cited 2024 Jun 29];10(8). Available from: https://pubmed.ncbi.nlm.nih.gov/35918123/

66. Jiang K, Song X, Yang L, Li L, Wan Z, Sun X, et al. Enhanced antitumor and anti-metastasis efficacy against aggressive breast cancer with a fibronectin-targeting liposomal doxorubicin. Journal of Controlled Release. 2018 Feb 10;271:21–30.

67. Oh E, Pierschbacher M, Ruoslahti E. Medical Sciences Deposition of plasma fibronectin in tissues (extracellular matrix/basement membranes/plasma proteins). 1981 [cited 2024 May 13];78(5):3218–21. Available from: https://www.pnas.org

68. Lin TC, Yang CH, Cheng LH, Chang WT, Lin YR, Cheng HC. Fibronectin in Cancer: Friend or Foe. Cells [Internet]. 2020 Jan 1 [cited 2024 May 13];9(1). Available from: /pmc/articles/PMC7016990/

69. Giancotti FG, Ruoslahti E. Integrin Signaling. [cited 2024 May 13]; Available from: https://www.science.org

70. Longstreth JH, Wang K. The role of fibronectin in mediating cell migration. Am J Physiol Cell Physiol [Internet]. 2024 Apr 1 [cited 2024 Jun 29];326(4):C1212–25. Available from: https://pubmed.ncbi.nlm.nih.gov/38372136/

71. Oudin MJ, Jonas O, Kosciuk T, Broye LC, Guido BC, Wyckoff J, et al. Tumor cell–driven extracellular matrix remodeling drives haptotaxis during metastatic progression. Cancer Discov [Internet]. 2016 May 1 [cited 2024 Jul 15];6(5):516–31. Available from: /cancerdiscovery/article/6/5/516/5516/Tumor-Cell-Driven-Extracellular-Matrix-Remodeling

72. A small-molecule RGD-integrin antagonist inhibits cell adhesion, cell migration and induces anoikis in glioblastoma cells [Internet]. [cited 2024 May 13]. Available from: https://www.spandidos-publications.com/ijo/42/1/83

73. Winkler J, Abisoye-Ogunniyan A, Metcalf KJ, Werb Z. Concepts of extracellular matrix remodelling in tumour progression and metastasis. Nat Commun [Internet]. 2020 Dec 1 [cited 2023 Aug 15];11(1). Available from: /pmc/articles/PMC7547708/

74. Farrar CS, Hocking DC. Assembly of fibronectin fibrils selectively attenuates platelet-derived growth factor–induced intracellular calcium release in fibroblasts. J Biol Chem [Internet]. 2018 Nov 11 [cited 2024 Jul 14];293(48):18655. Available from: /pmc/articles/PMC6290149/

75. He J, Steffen JH, Thulstrup PW, Pedersen JN, Sauerland MB, Otzen DE, et al. Anastellin impacts on the processing of extracellular matrix fibronectin and stimulates release of cytokines from coronary artery smooth muscle cells. Scientific Reports 2022 12:1 [Internet]. 2022 Dec 21 [cited 2024 Jul 14];12(1):1–15. Available from: https://www.nature.com/articles/s41598-022-26359-9

76. Belitškin D, Pant SM, Munne P, Suleymanova I, Belitškina K, Hongisto H, et al. Hepsin regulates TGFβ signaling via fibronectin proteolysis. EMBO Rep [Internet]. 2021 Nov 11 [cited 2024 Jul 14];22(11). Available from: /pmc/articles/PMC8567232/

77. Wei L, Chen Q, Zheng Y, Nan L, Liao N, Mo S. Potential Role of Integrin α5β1/Focal Adhesion Kinase (FAK) and Actin Cytoskeleton in the Mechanotransduction and Response of Human Gingival Fibroblasts Cultured on a 3-Dimension Lactide-Co-Glycolide (3D PLGA) Scaffold. Med Sci Monit [Internet]. 2020 Feb 8 [cited 2024 Jul 14];26:e921626-1. Available from: /pmc/articles/PMC7027369/

78. Levkau B, Herren B, Koyama H, Ross R, Raines EW. Caspase-mediated Cleavage of Focal Adhesion Kinase pp125 FAK and Disassembly of Focal Adhesions in Human Endothelial Cell Apoptosis. J Exp Med [Internet]. 1998 [cited 2024 Apr 27];187(4):579–86. Available from: http://www.jem.org

79. Hadden HL, Henke CA. Induction of Lung Fibroblast Apoptosis by Soluble Fibronectin Peptides. https://doi.org/101164/ajrccm16242001015 [Internet]. 2012 Dec 14 [cited 2024 Apr 27];162(4 I):1553–60. Available from: www.atsjournals.org

80. Frisch SM, Vuori K, Ruoslahti E, Chan-Hui Y, Bristol *, Squibb M. Control of Adhesion-dependent Cell Survival by Focal Adhesion Kinase. [cited 2024 Jul 14]; Available from: http://rupress.org/jcb/article-pdf/134/3/793/1480423/793.pdf

81. Gilmore AP, Metcalfe AD, Romer LH, Streuli CH. Integrin-Mediated Survival Signals Regulate the Apoptotic Function of Bax through Its Conformation and Subcellular Localization. Journal of Cell Biology [Internet]. 2000 Apr 17 [cited 2024 Jul 14];149(2):431–46. Available from: http://www.jcb.org

82. Ko Ili DŠ, Almeida EAC, Schlaepfer DD, Dazin P, Aizawa S, Damsky CH, et al. Extracellular Matrix Survival Signals Transduced by Focal Adhesion Kinase Suppress p53-mediated Apoptosis. J Cell Biol [Internet]. 1998 [cited 2024 Jul 14];143(2):547–60. Available from: http://www.jcb.org

83. Kabir J, Lobo M, Zachary I. Staurosporine induces endothelial cell apoptosis via focal adhesion kinase dephosphorylation and focal adhesion disassembly independent of focal adhesion kinase proteolysis. Biochemical Journal [Internet]. 2002 Oct 10 [cited 2024 Jul 14];367(Pt 1):145. Available from: /pmc/articles/PMC1222856/?report=abstract

84. Hazlehurst LA, Argilagos RF, Emmons M, Boulware D, Beam CA, Sullivan DM, et al. Cell Adhesion to Fibronectin (CAM-DR) Influences Acquired Mitoxantrone Resistance in U937 Cells. Cancer Res [Internet]. 2006 [cited 2024 Jul 14];66(4):2338–83. Available from: http://aacrjournals.org/cancerres/article-pdf/66/4/2338/2558035/2338.pdf

85. Ye Y, Zhang R, Feng H. Fibronectin promotes tumor cells growth and drugs resistance through a CDC42-YAP-dependent signaling pathway in colorectal cancer. Cell Biol Int [Internet]. 2020 Sep 1 [cited 2024 Jul 14];44(9):1840–9. Available from: https://onlinelibrary.wiley.com/doi/full/10.1002/cbin.11390

86. Nakagawa Y, Nakayama H, Nagata M, Yoshida R, Kawahara K, Hirosue A, et al. Overexpression of fibronectin confers cell adhesion-mediated drug resistance (CAM-DR) against 5-FU in oral squamous cell carcinoma cells. Int J Oncol [Internet]. 2014 Apr [cited 2024 Jul 14];44(4):1376–84. Available from: https://pubmed.ncbi.nlm.nih.gov/24452447/

87. Polydorou C, Mpekris F, Papageorgis P, Voutouri C, Stylianopoulos T. Pirfenidone normalizes the tumor microenvironment to improve chemotherapy. 2017 [cited 2023 Jul 24];8(15):24506–17. Available from: www.impactjournals.com/oncotarget